Sustainable Technologies
EVALUATION PROGRAM

Geothermal-based Thermal Mitigation of Stormwater Retention Pond Outflows

Report Addendum

Prepared by:

Toronto and Region Conservation Authority

Prepared for:

City of Brampton

November 2021

PUBLICATION INFORMATION

Citation: Erik Janssen and Tim Van Seters. 2021. *Geothermal-based Thermal Mitigation of Stormwater Retention Pond Outflows: Report Addendum*. Sustainable Technologies Evaluation Program, Toronto and Region Conservation Authority, Vaughan, Ontario.

Documents prepared by the Sustainable Technologies Evaluation Program (STEP) are available at www.sustainabletechnologies.ca. For more information about this or other STEP publications, please contact:

Tim Van Seters
Manager, STEP
Toronto and Region Conservation Authority
101 Exchange Avenue
Vaughan, Ontario
E-mail: tim.vanseters@trca.ca

Erik Janssen
Analyst, STEP
Toronto and Region Conservation Authority
101 Exchange Avenue
Vaughan, Ontario
E-mail: erik.janssen@trca.ca

THE SUSTAINABLE TECHNOLOGIES EVALUATION PROGRAM

The Sustainable Technologies Evaluation Program (STEP) is a multi-agency initiative developed to support broader implementation of sustainable technologies and practices within a Canadian context. STEP works to achieve this overarching objective by:

- Carrying out research, monitoring and evaluation of clean water and low carbon technologies;
- Assessing technology implementation barriers and opportunities;
- Developing supporting tools, guidelines and policies;
- Delivering education and training programs;
- Advocating for effective sustainable technologies; and
- Collaborating with academic and industry partners through our Living Labs and other initiatives.

Technologies evaluated under STEP are not limited to physical devices or products; they may also include preventative measures, implementation protocols, alternative urban site designs, and other innovative practices that help create more sustainable and livable communities.

ACKNOWLEDGEMENTS

Support for this project was provided by the City of Brampton. Additional funding support is provided to STEP by the City of Toronto, York Region and the Region of Peel.

PROJECT TEAM

The STEP team included:

- Erik Janssen, Analyst
- Tim Van Seters, Senior Manager
- Ricardo Brown, Technician
- Leigh St. Hilaire, Project Manager
- David Nixon, Advisor
- Svend De Bruyn, Advisor
- Mark Hummel, Technician
- Dean Luciani, Technician
- Gil Amdurski, Technical Coordinator
- Christy Graham, Coordinator

NOTICE

The contents of this report do not necessarily represent the policies of the supporting agencies. Although every reasonable effort has been made to ensure the integrity of the report, the supporting agencies do not make any warranty or representation, expressed or implied, with respect to the accuracy or completeness of the information contained herein. Mention of trade names or commercial products does not constitute endorsement or recommendation of those products.

EXECUTIVE SUMMARY

This document is an addendum to the report *Geothermal-based Thermal Mitigation of Stormwater Retention Pond Outflows: Interim Report* released April 2020 and available on sustainabletechnologies.ca, which describes the design, modeling, implementation, and data monitoring of a small-scale pilot geothermal-based thermal management solution for a stormwater retention pond in Brampton, ON, during Summer 2019. This addendum provides additional monitoring and analysis for Summer 2020 when 50% propylene glycol was used as the heat transfer fluid instead of water. The glycol replaced water in Fall 2019 and was required to freeze protect the system for winter temperatures. Note this was a one-time change and that the propylene glycol was also used as the heat transfer fluid moving forward, including Summer in 2020.

In Summer 2020, analysis of the monitoring data showed that glycol caused an increase in the thermal resistance for both the ground and stormwater heat exchangers (Table A). These are key parameters impacting system cooling capacity. The increase in thermal resistance caused a large reduction in overall cooling capacity for the system. The reduction in performance varied with the stormwater outflow temperature (the reduction being smallest at warmer temperatures) and was on the scale of 20% to 40%. The data was used to calibrate a physics-based system model. A comparison of modeled and measured geothermal cooling capacity showed that the model was an accurate predictor. The model was then used to evaluate the impact of different system sizes on the stormwater temperatures downstream of the geothermal system.

Table A. Change in heat exchanger thermal resistances between water and glycol heat transfer fluids.

	Water	**50% Glycol**
R_{SHX} [m°C/W]	0.17	0.17 – 0.27
R_{GHX} [m°C/W]	0.21	0.25

The impact of the glycol solution was less pronounced on the overall system sizing (Figure A). In Summer 2020, a geothermal system consisting of 10 deep vertical boreholes could keep outflow temperatures below 24°C for 91% of the time if using glycol, and 95% of the time if using water as the heat transfer fluid. With no geothermal, the pond outflow temperatures would be below 24 °C only 25% of the time during Summer 2020. In Summer 2019, approximately 6 deep vertical boreholes would keep outflow temperatures below 24 °C 97% of the time when using water as the heat transfer fluid, and 95% when using glycol. in summary, this addendum showed a small decrease in performance (from the perspective of system sizing) when using a glycol heat transfer fluid that could ultimately be rectified through larger component sizing.

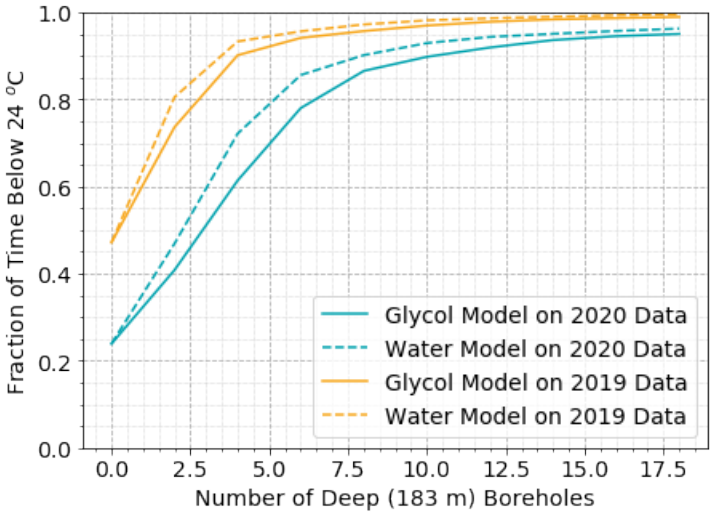

Figure A. The system model was used to evaluate the impact of geothermal system sizing on the stormwater outflow temperatures.

As outlined in the *Interim Report*, the need remains for additional thermal mitigation measures to keep outflows within target values a greater percentage of the time. Infiltration, in particular, requires re-examining. The modeling in this addendum showed that the floor and walls of the concrete vault containing the stormwater heat exchanger provided a notable amount of cooling. This is because the vault is in contact with the cooler subsurface ground and the interior of the vault is also shaded from solar radiation. These two features allow a vault to be potentially more impactful at cooling than rock-filled cooling trenches that are often deployed. In a sense, the vault is also providing "geothermal" cooling in that it is transferring heat from the stormwater to the subsurface ground, just that the vault is "passive" (no hydronics or pumping) and there is a smaller temperature differential (between stormwater and subsurface ground) to drive heat transfer.

For a concrete vault to provide to a significant level of cooling it would need to be several times larger than the vault installed at the pilot pond, and this may not be feasible due to either space or cost constraints. However, a large underground infiltration chamber could have a similar cooling impact to a vault, in addition to infiltrating the stormwater. When considering an infiltration chamber, the *Interim Report* concluded that such a chamber would need to be prohibitively large to make a significant impact on the thermal load and that the other measures considered, longer drawdown times and subsurface draw, would be more impactful. This needs re-examination. The *Interim Report* only considered the impact of an infiltration chamber mitigating the flowrates from the pond. It did not consider passive heat transfer between the warm stormwater and the cooler subsurface ground (like that occurring in the vault). The latter factor may be the most important regarding thermal mitigation. This should be considered in future work.

Overall, in the landscape of thermal mitigation technologies, an "active" geothermal system like that studied in this project offers something unique. Amongst other benefits, it can provide a large amount of cooling capacity in a small volume. It is also an approach that is highly adaptable to the existing site constraints. For example, a stormwater heat exchanger could be installed within the aggregate of an underperforming cooling trench, or similarly it could be installed in a stormwater outflow pipe. For similar reasons, active geothermal ought to integrate well with other thermal mitigation measures in the context of both an existing pond and in a new pond.

Passive systems without mechanical components are normally preferred, but they may not always be feasible or may not have sufficient cooling capacity to meet target outflow temperatures. In those circumstances, this pilot has demonstrated that geothermal offers a compelling option. Additional considerations on system improvements, sizing, future work, and other topics are available in the *Interim Report*.

CONTENTS

1.0 Introduction 1
2.0 Analysis 2
2.1 System Model Review 2
2.2 Analysis Overview 5
3.0 Results 6
3.1 Stormwater Temperatures, Flowrates, and Overall Thermal Load 6
3.2 Cooling Capacities 8
3.3 Ground Temperature Model 8
3.4 Thermal Resistance of GHX 9
3.5 Thermal Resistance of SHX 14
3.6 Additional Flowrate and Thermal Resistance Considerations 17
3.7 System Model Summer 2020 18
3.8 System Sizing 23
4.0 Discussion 24
5.0 Conclusion 26

1.0 INTRODUCTION

This report is an addendum to the report *Geothermal-based Thermal Mitigation of Stormwater Retention Pond Outflows: Interim Report* released April 2020 and available on sustainabletechnologies.ca, which describes the design, modeling, implementation, and data monitoring for a small-scale pilot of a geothermal-based thermal management solution for a stormwater retention pond in Brampton, ON, during Summer 2019.

This addendum provides additional monitoring and analysis for Summer 2020 when 50% propylene glycol was used as the heat transfer fluid instead of water. The glycol replaced water in Fall 2019 and was required to freeze protect the system for winter temperatures. Note this was a one-time change and that the propylene glycol continued to be used as the heat transfer fluid during Summer 2020 and moving forward.

Introductory information about the system and site is provided in the *Interim Report* and has not been duplicated here. However, Section 5.0 from the *Interim Report,* which provides the equations used in the analysis and the system model, has been largely duplicated in this addendum within Section 2.0 because the equations required frequent referencing.

2.0 ANALYSIS

2.1 System Model Review

A simple model of the geothermal-based thermal mitigation system is shown in Figure 2-1. The system is a hydronic circuit where piping connects a stormwater heat exchanger to a ground heat exchanger. A pump circulates a heat transfer fluid through the hydronic circuit. At the SHX, the heat transfer fluid is cooler than the warm stormwater outflows. This temperature difference drives heat from the stormwater and into the heat transfer fluid, cooling the stormwater in the process. At the GHX, the heat transfer fluid is warmer than the deep ground. This temperature difference drives heat from the heat transfer fluid into the deep ground, cooling the fluid to its original temperature. This cycle can be used to continuously cool the warm stormwater.

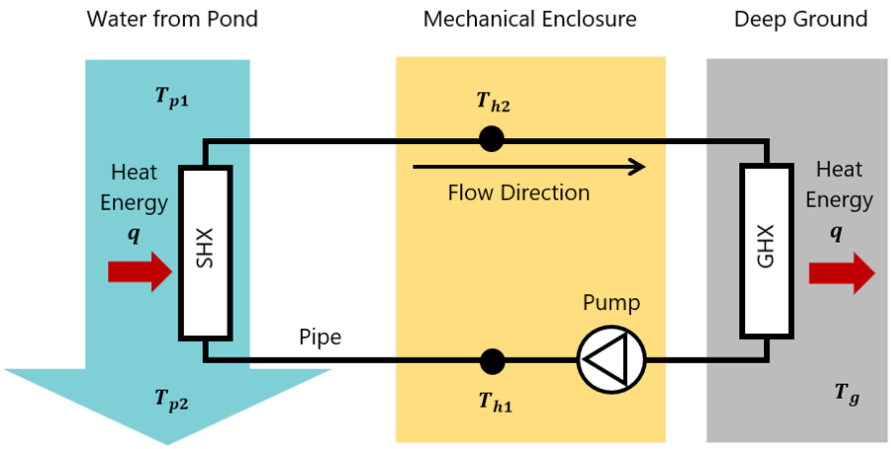

Figure 2-1. Schematic of the geothermal-based thermal mitigation system.

Figure 2-1 shows the temperatures for different parts of the system. They are described further below:

- T_{p1} is the stormwater outflow temperature upstream of the SHX;
- T_{p2} is the stormwater outflow temperature downstream of the SHX;
- T_g is the deep ground temperature in the vicinity of the borehole;
- T_{h1} is the heat transfer fluid temperature leaving the GHX and entering the SHX;
- T_{h2} is the heat transfer fluid temperature leaving the SHX and entering the GHX.

The heat transfer (q_r) required to cool a given stormwater flowrate is given in Equation 1, where ρ_p is the density of water, F_p is the flowrate of the stormwater from the pond, and C_p is the specific heat capacity of water. Note that Equation 1 also describes the amount of cooling occurring for arbitrary values T_{p1} and T_{p2}. It becomes the "required" cooling when a desired set-point value of T_{p2} is used in the equation.

$$q_r = \rho_p \cdot F_p \cdot C_p \cdot (T_{p1} - T_{p2}) \qquad \textbf{Equation 1}$$

The heat transfer to the SHX (q_{SHX}) can be described by Equation 2.[1] In this equation, the SHX is assumed to be composed of HDPE pipe because that was what used in the STEP pilot. A stainless-steel plate heat exchanger is an option as well and this would require a slight adjustment of the equation. Note that L_{SHX} is the length of the SHX, R_{SHX} is the thermal resistance, and $LMTD_{SHX}$ is the log mean temperature difference driving the heat transfer.

$$q_{SHX} = \left(\frac{L_{SHX}}{R_{SHX}}\right) \cdot LMTD_{SHX} \quad \textbf{Equation 2}$$

$$LMTD_{SHX} = \left[\frac{T_{p1}+T_{p2}}{2} - T_{h2} - \left(\frac{T_{p1}+T_{p2}}{2} - T_{h1}\right)\right] \cdot \left[ln\left(\frac{\frac{T_{p1}+T_{p2}}{2} - T_{h2}}{\frac{T_{p1}+T_{p2}}{2} - T_{h1}}\right)\right]^{-1} \quad \textbf{Equation 3}$$

The heat transfer to the ground (q_{GHX}) can be described by Equation 4,[2] where L_{GHX} is the total borehole length (depth of boreholes multiplied number of boreholes) and R_{GHX} is the thermal resistance. Defining L_{GHX} as one long length might seem to ignore the fact that the GHX may be composed of many boreholes which could have both series and parallel connections. However, it's straightforward to show that multiple boreholes connected in parallel can be described as one long borehole length provided the boreholes are spaced far enough apart that interactions between adjacent boreholes can be neglected.

$$q_{GHX} = \left(\frac{L_{GHX}}{R_{GHX}}\right) \cdot \left(\frac{T_{h1}+T_{h2}}{2} - T_g\right) \quad \textbf{Equation 4}$$

In a steady-state where the system is exactly meeting the load, Equation 5 holds true.

$$q_r = q_{SHX} = q_{GHX} = q \quad \textbf{Equation 5}$$

The relationship between T_{h1} and T_{h2} is defined by the heat transfer and the hydronic flow rate of the system according to Equation 6. In this equation, ρ_h is the density of the heat transfer fluid, F_h is the heat transfer fluid flow rate, and C_h is the heat transfer fluid specific heat capacity. The heat transfer fluid may be water, an ethanol solution, or a propylene glycol solution. These solutions are all non-toxic. Note that T_{h1} can't drop below T_g.

$$T_{h1} = T_{h2} - \frac{q}{\rho_h \cdot F_h \cdot C_h} \quad \textbf{Equation 6}$$

Substituting Equation 6 into Equation 4 yields Equation 7 which can used to solve for a value of T_{h2} provided all other parameters are defined. It is then possible to find the value of T_{h1}. Putting all these equations together yields Equation 8 which describes the system as a whole.

$$T_{h2} = q \cdot \left(\frac{R_{GHX}}{L_{GHX}}\right) + \frac{q}{2 \cdot \rho_h \cdot F_h \cdot C_h} + T_g \quad \textbf{Equation 7}$$

$$0 = \left(\frac{L_{SHX}}{R_{SHX}}\right) \cdot LMTD_{SHX} - \left(\frac{L_{GHX}}{R_{GHX}}\right) \cdot \left(\frac{T_{h1}+T_{h2}}{2} - T_g\right) \quad \textbf{Equation 8}$$

[1] Equation 5.6 in Kavanaugh, Steve and Rafferty, Kevin. "Geothermal Heating and Cooling: Design of Ground-source Heat Pump Systems."ASHRAE, 2014.

[2] Equation 3.1 in Kavanaugh, Steve and Rafferty, Kevin. 2014.

Equation 8 can be more simply expressed as Equation 9 (ignoring the physical constants for density and specific heat capacity). Note that T_{h1} and T_{h2} are not parameters of the model but are instead calculated quantities from these other more fundamental parameters.

$$0 = f(T_{p1}, T_{p2}, F_p, F_h, R_{GHX}, R_{SHX}, L_{GHX}, L_{SHX}, T_g) \quad \textbf{Equation 9}$$

Lastly, note that the cooling capacity of the system could also be determined from the monitoring data based on the change in heat transfer fluid temperature across the SHX and GHX and the hydronic flowrate. This shown in Equation 10 where, where ρ_h is the density of the heat transfer fluid, F_h is the flowrate of the heat transfer fluid through the closed circuit, and C_h is the specific heat capacity of the heat transfer fluid.

$$q_h = \rho_h \cdot F_h \cdot C_h \cdot (T_{h2} - T_{h1}) \qquad \textbf{Equation 10}$$

2.2 Analysis Overview

The primary objective of the analysis was to compare the performance of the geothermal-based thermal mitigation system when using the 50% glycol heat transfer fluid (in Summer 2020) against the performance of the system when using water (in Summer 2019), and ultimately the impact of the heat transfer fluid on the sizing of a full-scale system. The analysis proceeded as follows:

1. The stormwater temperatures, flowrates, and overall thermal load were for Summer 2019 and Summer 2020 were compared.
2. The overall cooling capacities of the system for Summer 2019 and Summer 2020 were compared.
3. The ground temperature model from Summer 2019 was applied to Summer 2020 and compared against the actual ground temperature measurements taken in Summer 2020.
4. The thermal resistance of the ground heat exchanger and the stormwater heat exchanger (R_{SHX} and R_{GHX}) were calculated for Summer 2020 and compared against the results from Summer 2019.
5. The calibrated system model for Summer 2020 was used to predict the pond outflow temperatures and compared against the measured values.
6. The system sizing procedure was completed using the calibrated model from Summer 2020 and compared against the result from Summer 2019.

3.0 RESULTS

3.1 Stormwater Temperatures, Flowrates, and Overall Thermal Load

The stormwater temperatures, flowrates and overall thermal load (to cool pond outflows to 24 °C) are shown in Figure 3-1 to Figure 3-3, respectively. Summer 2020 had a much greater thermal load than Summer 2019. The outflow temperatures were generally warmer and the stormwater flow from the pond was much greater during July/August. Figure 3-4 shows the results from the machine learning pond model from the *Interim Report* which predicted the thermal load based the environmental data from previous years (2013 – 2018). The thermal load from the pond in Summer 2020 was also high in comparison to these years.

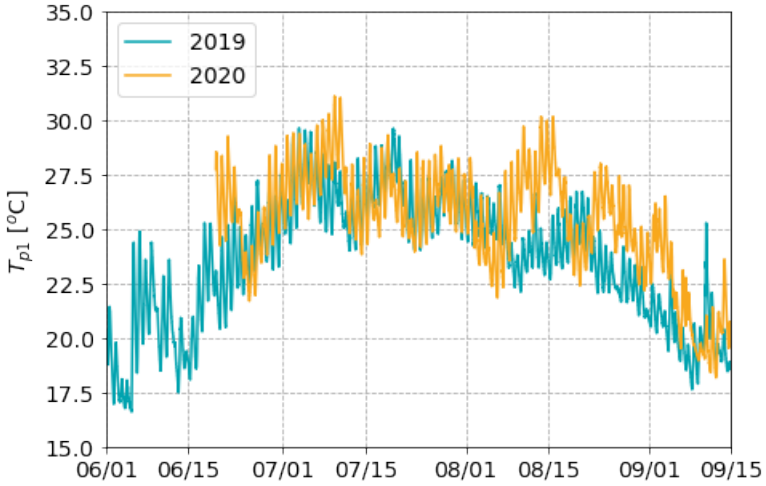

Figure 3-1. The pond outflow temperatures upstream of the SHX (T_{p1}) were typically warmer in 2020 compared to 2019.

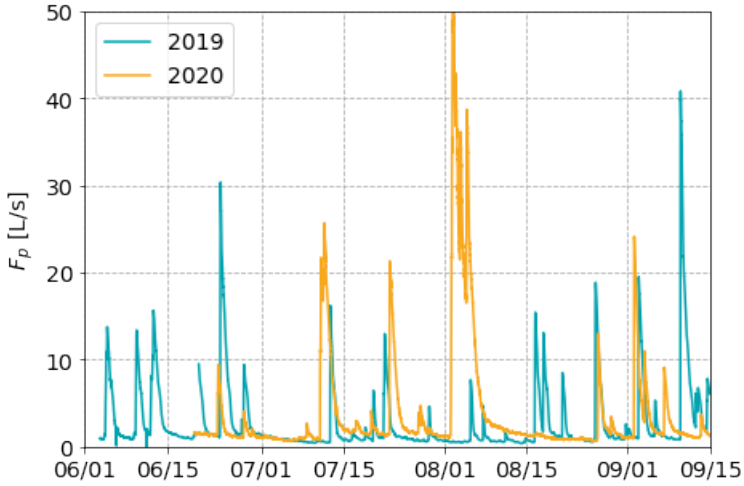

Figure 3-2. The outflows from the pond during July and August (when the outflow temperatures are warmest) were much greater in 2020 than in 2019.

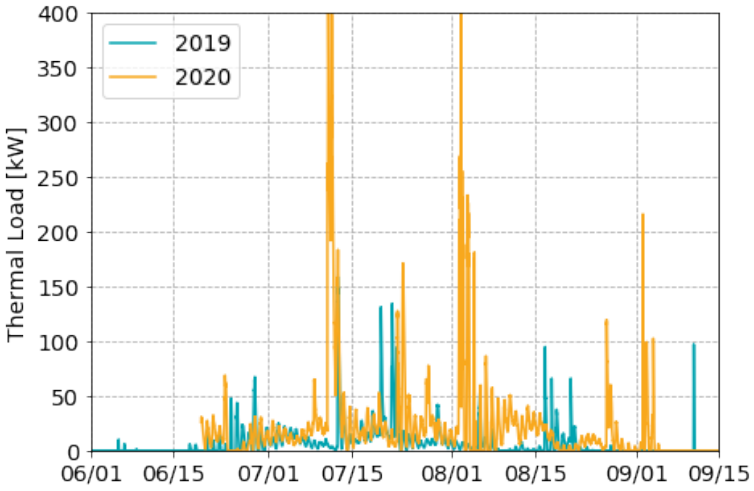

Figure 3-3. The outflow temperatures and flowrates were combined to calculate the total thermal load to reduce the outflow temperature to 24 °C. The overall thermal load in 2020 was much greater than in 2019.

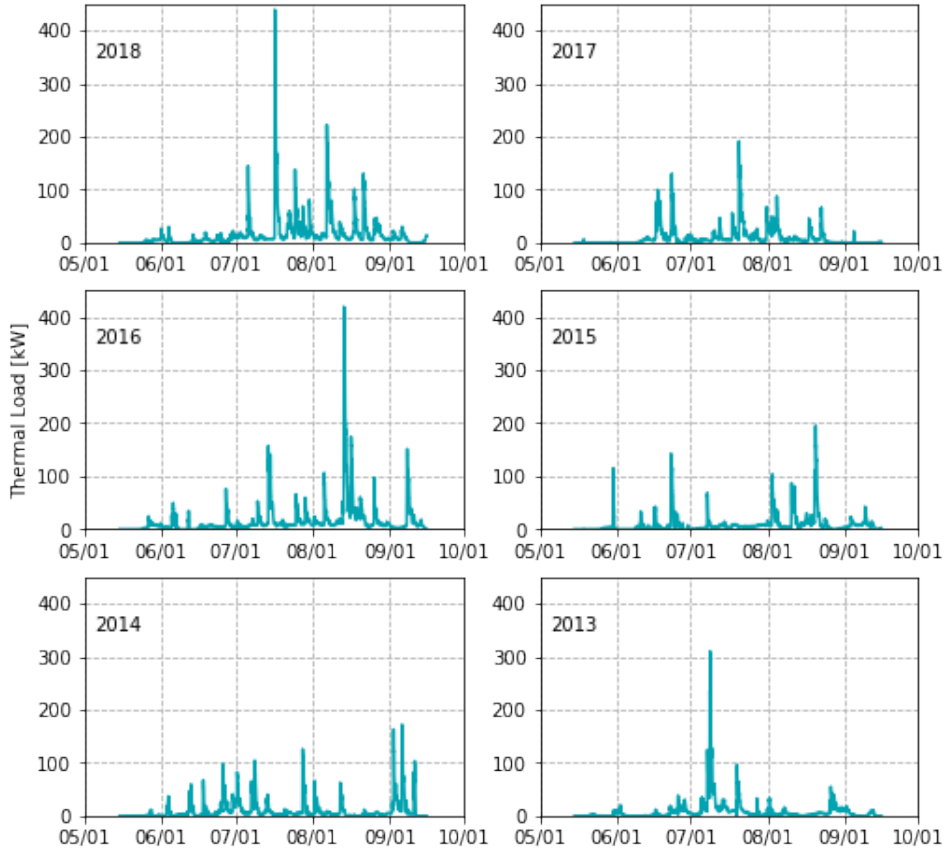

Figure 3-4. The *Interim Report* used machine learning modelling of the pond to predict the thermal load of the pond from 2013 to 2018 based on environmental data. Summer 2020 stands out as having a high thermal load.

3.2 Cooling Capacities

The cooling capacity of the geothermal system was calculated from the heat gain of the glycol flowing through the SHX (Equation 10) and noting that the specific heat capacity and density of the glycol solution for the working temperatures of the system during the summer were 3,698 J/(kg°C) and 1,044 kg/m^3 respectively[3] (whereas these parameters for water are 4,186 J/(kg°C) and 1,000 kg/m^3).

Figure 3-5 shows the cooling capacity of the system as a function of the stormwater outflow temperature for both 2019 and 2020. The system has a lower cooling capacity when using 50% propylene glycol as the heat transfer fluid. However, the relative difference in the cooling capacity between the two different heat transfer fluids reduces with warmer outflow temperatures (i.e. the point clouds are spread apart when the outflow temperature is 22 °C, but closer together when it approaches 30 °C). The reduction in system performance appears close to 40% when the outflow temperatures are near 22 °C but it reduces to closer to 20% near 30 °C.

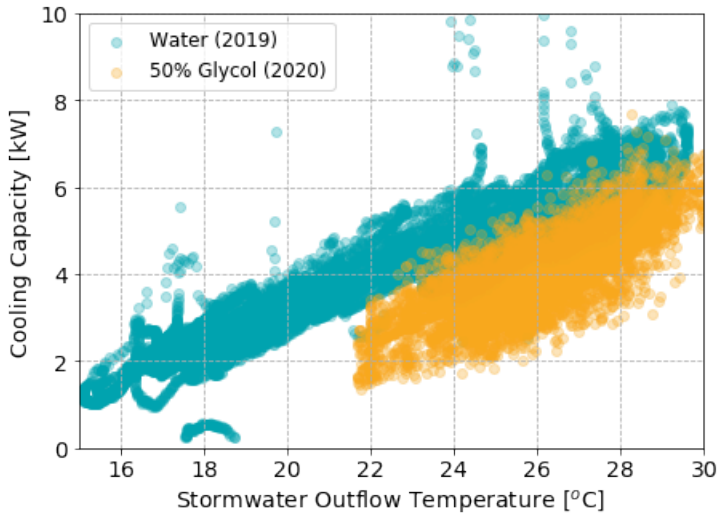

Figure 3-5. The cooling capacity of the system is lower when using 50% propylene glycol as the heat transfer solution.

3.3 Ground Temperature Model

The ground temperature model derived from Summer 2019 was applied to Summer 2020 data. This is shown in Figure 3-6. *Actual* is from an actual ground temperature measurement where the system was turned off for several days to allow the heat transfer fluid to equilibrate to the ground temperature. Then the system was turned back on and the temperatures of the heat transfer fluid coming out of the borehole gave an indication of the ground temperature.

Modeled is the ground temperature model derived from Summer 2019 fit to the Summer 2020 data. Recall from the *Interim Report* that the model considers ground temperature increases due to heat begin rejected to the ground from

[3] Dynalene. Dynalene Propylene Glycol Engineering Guide. 2020. Accessed online June 2021: https://www.dynalene.com/wp-content/uploads/2020/05/Dynalene-PG-engineering-guide.pdf. Note that all glycol data was taken form this Engineering Guide.

the borehole, and temperatures decreases due to heat being dissipated to the far ground. Overall, the agreement is good.

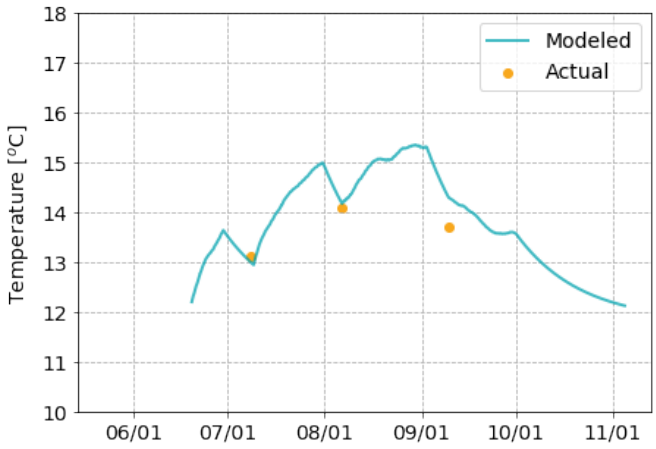

Figure 3-6. The ground temperature model derived from Summer 2019 was applied to Summer 2020 data and compared against ground temperature measurements which were periodically taken across the summer. The agreement is overall good.

3.4 Thermal Resistance of GHX

R_{GHX} was calculated for the 2020 data in the same way as with the 2019 data – using data taken after a ground temperature measurement when the system had shut been shut off for several days to equilibrate with the ground temperature. R_{GHX} can be determined from the slope of the lines shown in Figure 3-7. In 2019, only one of the ground temperature measurements was conducted by turning off the system entirely, so the data set is smaller. In 2020, this was done three times. In 2019, the heat transfer of coefficient of the borehole was 859 W/°C which corresponds to an R_{GHX} of 0.21 m°C/W (by taking the inverse of the slope and multiplying by the borehole length of 183 m). In 2020, with the propylene glycol solution, R_{GHX} was 0.28 m°C/W on average.

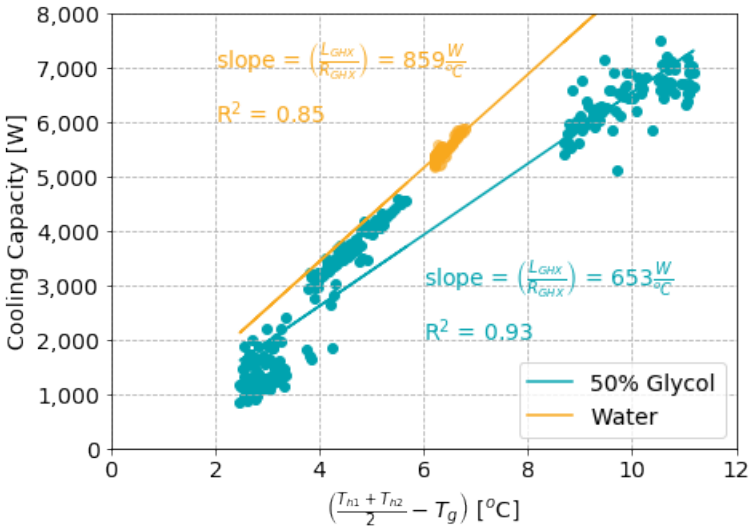

Figure 3-7. There is a linear relationship between the cooling capacity and the temperature difference between the deep ground and the average hydronic temperature in the borehole. The slope is inversely proportion to thermal resistance. It follows that the lower slope with 50% propylene glycol means that the thermal resistance is greater.

While R^2 is good, Figure 3-7 shows that there is notable variation between the data collected after each ground temperature measurement (shown as the different clusters of points). Using the ground temperature model from Figure 3-6, it is possible to evaluate R_{GHX} in a different way. Rearranging Equation 4 yields Equation 11. It can be used to visualize R_{GHX} as a time-series and also as a function of other system parameters to better understand what may be influencing it.

$$R_{GHX} = \left(\frac{L_{GHX}}{q_h}\right) \cdot \left(\frac{T_{h1} + T_{h2}}{2} - T_g\right) \qquad \textbf{Equation 11}$$

However, prior to plotting R_{GHX} against other system parameters, it was necessary to first aggregate the 5-min monitoring data to a longer time-scale. This is because the heat transfer equations are for a steady-state. There was a much larger variability over short timescales in the hydronic flowrate for Summer 2020 when using a glycol solution than there was with water. This variation pushed the system further from a steady-state over short timescales and reduced the validity of the governing equations on an instantaneous basis. Example data from a day in July 2019 and July 2020 is shown in Figure 3-8. The hydronic flowrate in 2019 tends to vary within ±0.5 L/min, that for 2020 tends to vary within ±2 L/min.

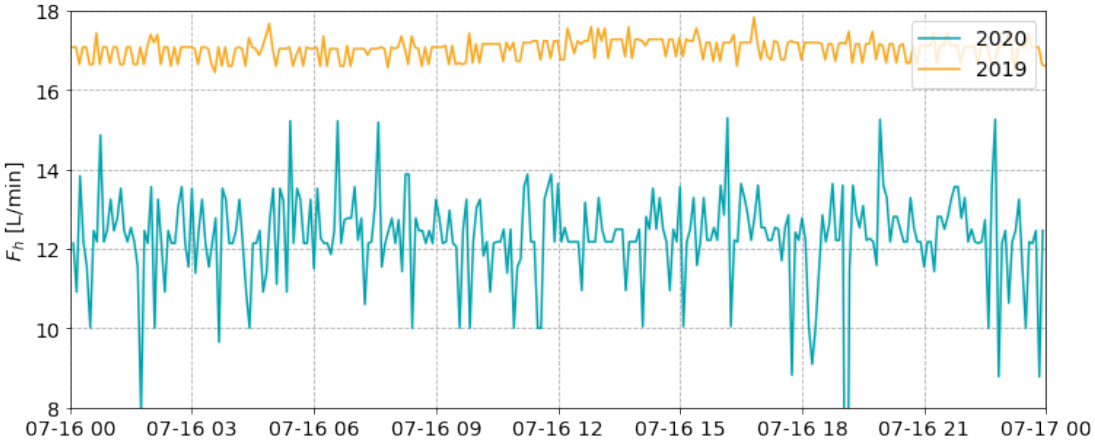

Figure 3-8. Greater variation in the hydronic flowrate data was seen in 2020 (with 50% glycol) than in 2019 (with water). This created comparable variation in the calculated cooling capacity.

The cause of the variation is related to the pressure of the hydronic system. In late July 2020, the research team noted that the system pressure was low. This could have been due to a small leak.[4] When the system was pressurized with additional glycol, the flowrate increased, and the variation was reduced to a comparable level as was seen in Summer 2019 (Figure 3-9). However, the problem returned in September and even greater variability in the readings was observed.

A time-series plot of thermal resistance (as calculated in Equation 11) is shown in Figure 3-10. Within the plot, data has been aggregated into 12-hr mean values to reduce the scatter shown in Figure 3-8 and better approximate a steady-state. The data suggests that R_{SHX} is 0.33 m°C/W on average in July and 0.25 m°C/W on average in August. Changes in R_{GHX} are correlated to the hydronic flowrate but not the glycol temperature. This is shown in Figure 3-11 and Figure 3-12.

[4] Note that the system was installed with a pressure switch to turn off the pump if the pressure reduced beyond a certain preset value. This would help to prevent large leaks. Also note that, insofar as was possible, joints and system connections were made in the mechanical enclosure sitting on top of the vault rather than inside the vault and in the path of the stormwater flow. Unless the HDPE pipe itself was severely damaged, a leak would need to originate from inside the mechanical enclosure where it would be contained.

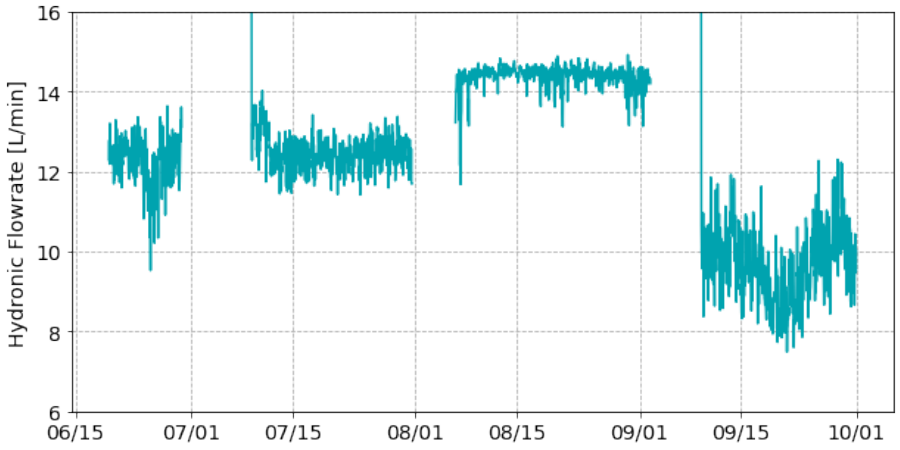

Figure 3-9. When the system pressure was increased in early August, the variability in the flowrate readings was greatly reduced and there was a small increase in the flowrate. However, the problem returned in September. Note that this data was aggregated on a 1 hr basis.

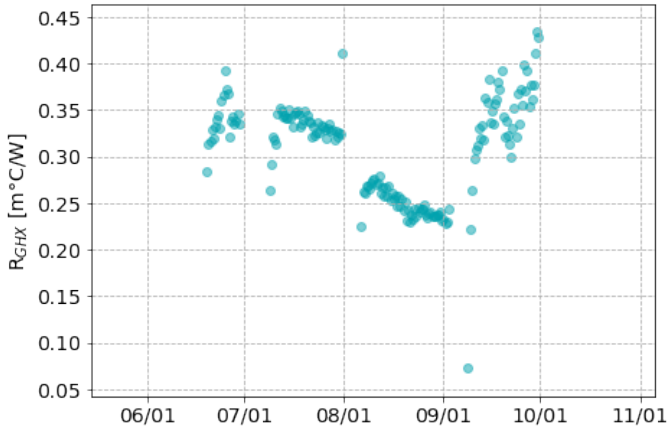

Figure 3-10. The ground temperature model results were used alongside the monitoring data to estimate R_{GHX} and it appeared not be a constant across the monitoring period.

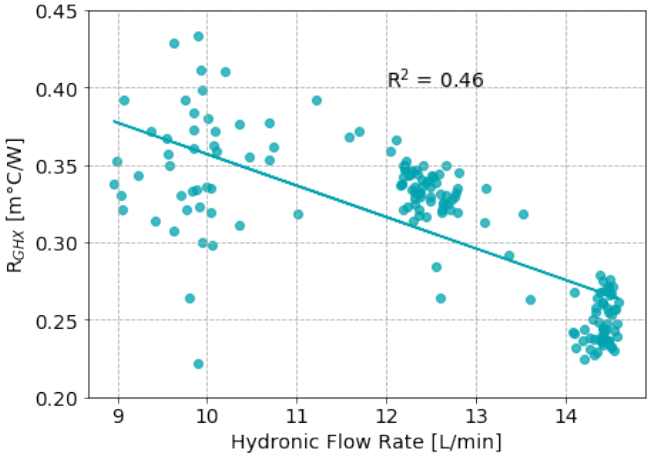

Figure 3-11. R_{GHX} appeared to be correlated to the hydronic flowrate.

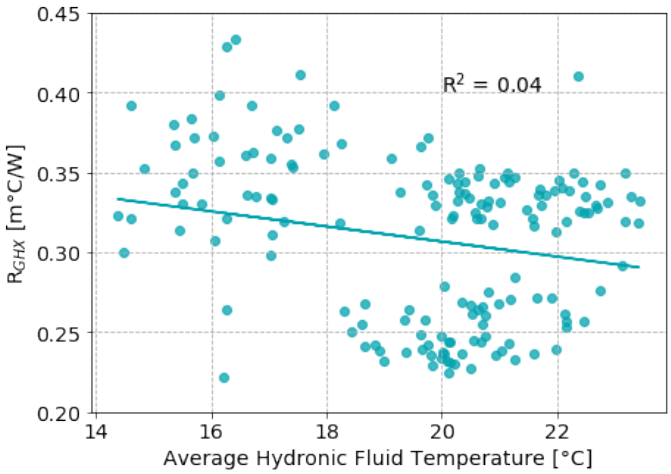

Figure 3-12. R_{GHX} did not appear to be correlated with the hydronic temperatures.

The approach to calculate R_{GHX} from Equation 11 was also applied to the Summer 2019 data when water was used as the heat transfer fluid. There is also clearly a correlation between R_{GHX} and hydronic flowrate when water was used. R_{GHX} was 0.21 m°C/W on average when the hydronic flowrate averaged 17.4 L/min – while it was 0.28 m°C/W on average when flowrate averaged 7.4 L/min. The lower flowrate was obtained when the pump was intentionally set to a lower speed.

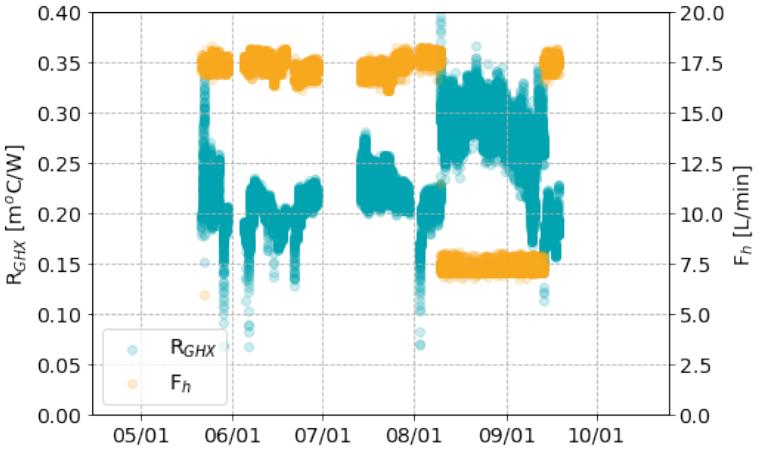

Figure 3-13. In Summer 2019, R_{GHX} was greater when a higher hydronic flowrate was used.

There are (at least) two key differences in the heat transfer properties of 50% propylene glycol versus those of water. Firstly, there is a large difference in thermal conductivity between the two fluids. The thermal conductivity of 50% glycol (0.36 W/(m°C) at the working temperatures of the system) is much poorer than that of water (0.598 W/(m°C)). This means that propylene glycol will conduct less heat than water given the same conditions. Secondly, the glycol solution is more viscous than water and this can significantly impact the flow regime within the pipe even if comparable flow rates were achieved.

The Reynold's number (Re) is useful to help understand the flow regime in the pipe. Laminar flow is characterized by a lack of mixing – such that conductive heat transfer within the heat transfer fluid becomes a key mechanism. Turbulent flow is characterized by a high degree of mixing which promotes better heat transfer. When Re is less than 2300 in a circular pipe the flow is laminar. Above 2300 is transitional and above 2900 is turbulent. Re is shown in Equation 12, where ρ_h is the heat transfer fluid density in units kg/m^3, F_h is the hydronic flowrate in units m^3/s, D_h is the pipe diameter, μ is the dynamic viscosity in units Pa s, and A is the cross-sectional area of the pipe in units m^2.

$$Re = \frac{\rho_h F_h D_h}{\mu A} \qquad \textbf{Equation 12}$$

Calculations of Re for the GHX with water and glycol are shown in Table 3-1. The calculations provide a potential explanation for the increase in thermal resistance of the GHX when switching from water to 50% glycol - the flow regime changed from transitional to laminar where poorer heat transfer is expected. This change was compounded by the fact that in a laminar flow regime, conduction is a primary mechanism of heat transfer within the heat transfer fluid and, as mentioned, the thermal conductivity of 50% glycol is poorer than that of water.

Table 3-1. Input parameter and calculations results for Reynold's number calculation of GHX

		ρ_h [kg/m^3]	F_h [m^3/s]	D_h [m]	μ [Pa s]	A [m^2]	**Re**	**Regime**	**R_{GHX} [m°C/W]**
1	**Water (17.4 L/min)**	998	0.000290	0.0340	0.00100	0.000907	**10,849**	**Turbulent**	**0.21**
2	**Water (7.4 L/min)**	998	0.000123	0.0340	0.00100	0.000907	**4,601**	**Turbulent**	**0.28**
3	**50% Glycol (14.4 L/min)**	1,043	0.000240	0.0340	0.00681	0.000907	**1,378**	**Laminar**	**0.25**
4	**50% Glycol (12.4 L/min)**	1,043	0.000207	0.0340	0.00681	0.000907	**1,188**	**Laminar**	**0.33**

*Values for 20 °C

However, flow regime does not help to explain why the increase in the glycol flowrate from 12.4 to 14.4 L/min is correlated with a drastic decrease in thermal resistance as shown in Figure 3-11. The flow regime in both cases was laminar and the change in flowrate was relatively small. Similarly, flow regime does not explain why thermal resistance decreased when using water as the heat transfer fluid and the flowrate decreased. Ultimately, further than the general observation that higher flowrates ought to improve heat transfer through greater convective heat transfer, the physical basis for the change in thermal resistance was not identified. System sizing used the lower thermal resistance value, while model verification used whichever value was more appropriate in trying to closely predict the downstream temperature.

3.5 Thermal Resistance of SHX

The same basic approach used to calculate thermal resistance in the GHX (shown in Figure 3-7) was used for the SHX. This is shown in Figure 3-14. In 2019, R_{SHX} was 0.17 m°C/W with water as the heat transfer fluid when the flowrate was 17.4 L/min and it was 0.20 m°C/W when the flowrate was 7.4 L/min. In 2020, it averaged 0.24 m°C/W overall. This was an increase up to 41%. The greater thermal resistance of both the SHX and GHX when using glycol partly explains why, in Figure 3-5, the cooling capacity is overall lower.

Notably, the average R_{SHX} (as determined from the slope of the fit line in Figure 3-14) in 2020 is a relatively poor representation of the heat transfer that is occurring. This is evident from the low value of R^2 indicating that much of the variation within the data is due to factors other than the LMTD. It's helpful to visualize R_{SHX} in a different way. R_{SHX} can also be determined for each monitoring interval by rearranging Equation 2 to yield Equation 13. It can then be plotted against other system parameters to better understand the factors influencing the variation of the data.

$$R_{SHX} = \left(\frac{L_{SHX}}{q_h}\right) \cdot LMTD_{SHX} \qquad \textbf{Equation 13}$$

Figure 3-15 shows R_{SHX} plotted against the average heat transfer fluid temperature (the average of T_{h1} and T_{h2}) with the data having been agreggated over 12-hr periods. It is clear that the heat transfer fluid temperature correlates significantly with R_{SHX}. This was not the case with water as the heat transfer fluid which, as shown by the high R^2 of the fit line in Figure 3-14, was a constant value across the heating season. A weak correlation between R_{SHX} and the hydronic flowrate was also observed (Figure 3-16).

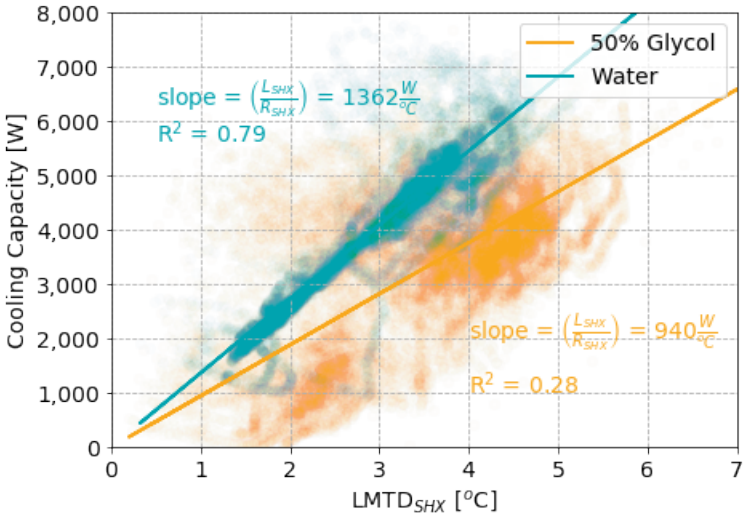

Figure 3-14. R_{SHX} can be found by plotting cooling capacity against LMTD. R_{SHX} is inversely proportional to the slope of a linear fit of the data. It is therefore greater for the glycol solution than with water.

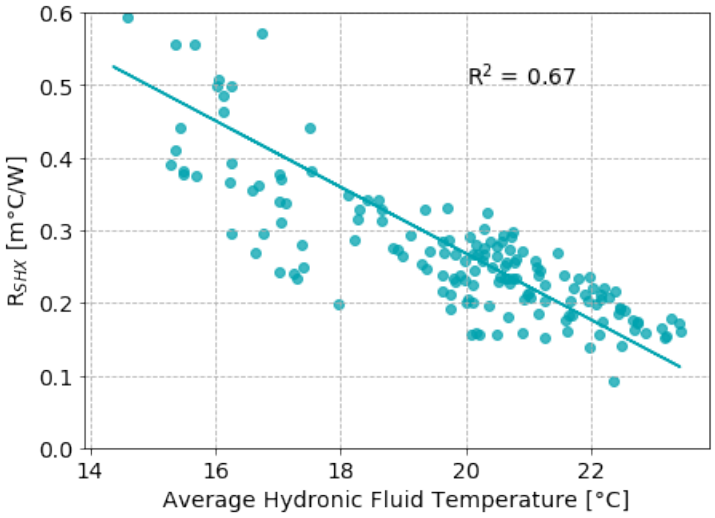

Figure 3-15. The thermal resistance of the SHX correlates with the average glycol temperature. As it approaches 24 °C, it appears to become similar to that achieved with water – which was 0.17 m°C/W (at higher flowrates).

There are different temperature-dependent parameters that may potentially impact heat transfer when using glycol – for example density, thermal conductivity, specific heat capacity, and viscosity – however the only one that varies greatly over this range of temperatures is the viscosity. All others vary less than 1%. At 14 °C the dynamic viscosity is 0.0085 Pa s while at 24 °C, it is 0.0057 Pa s. This is a reduction of 31%.

The viscosity can impact the fluid film thermal resistance on the inside of the pipe and the flow regime within the pipe. Re was calculated for the SHX in Table 3-2, considering 50% glycol at different temperatures and water. Recall that the SHX was split into 4 parallel circuits to reduce the pressure drop and it follows that flow rate was divided between 4 circuits as well, so it is much lower than in Table 3-1.

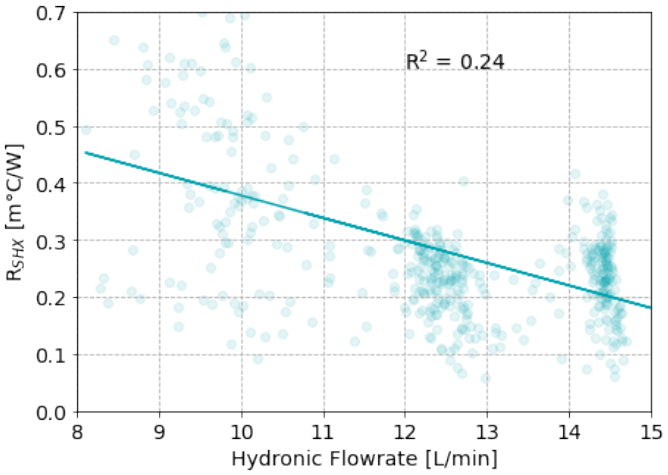

Figure 3-16. There is a weak correlation between hydronic flowrate and SHX thermal resistance.

Table 3-2. Input parameter and calculations results for Reynold's number calculation of the SHX

		ρ_h [kg/m^3]	F_h [m^3/s]	D_h [m]	μ [Pa s]	A [m^2]	**Re**	**Regime**
1	**Water (20 °C; 17.4 L/min)**	998	7.25e-5	0.0216	0.00100	0.000366	**4,270**	**Turbulent**
2	**50% Glycol (14 °C; 14.4 L/min)**	1,046	6.00e-5	0.0216	0.00848	0.000366	**437**	**Laminar**
3	**50% Glycol (24 °C; 14.4 L/min)**	1,041	6.00e-5	0.0216	0.00570	0.000366	**650**	**Laminar**

Table 3-2 provides an explanation for the increase in thermal resistance when switching from water to 50% glycol as the heat transfer fluid – the flow regime changed from turbulent to laminar. As noted with the GHX, the thermal conductivity of 50% glycol is much less than that of water as well. However, Table 3-2 does not explain the trend shown in Figure 3-15 since the flow regime did not change as the viscosity of glycol increased with temperature.

Presumably the strong correlation between the heat transfer fluid temperature and thermal resistance is related to viscosity as this is the parameter that has the greatest relative change over the short temperature interval being considered. However, heat transfer is complex, and the research team does not have a more detailed answer to offer. The overall aim of the exercise was to model the system's cooling performance and the relationship defined in Figure 3-15 is sufficient for this purpose, even if the physics behind the relationship have not been fully understood. However, note that the trend should not be extrapolated to the extent that the thermal resistance for 50% glycol would drop below that of water.

3.6 Additional Flowrate and Thermal Resistance Considerations

Another point to note is that, while the flowrate impacts system performance by way of the thermal resistance of the GHX and SHX, the system model also shows that flowrate impacts the system through other pathways. The sizing plot provided in the *Interim Report* (repeated below in Figure 3-17) showed that, for higher flowrates, less SHX is required – although the returns are diminishing. Essentially, this means that higher flowrates improve system performance, but the use of 50% propylene glycol reduced the flowrate by up to 30% (from 17.4 to 12.4 L/min during July until the pressure issue was fixed and the flow rate rose to 14.4 L/min in August).

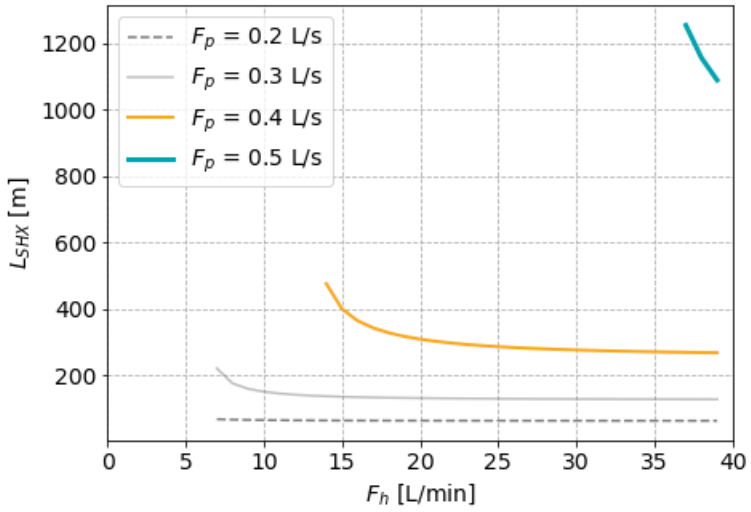

Figure 3-17. For greater hydronic flowrates (F_h), less SHX is required to cool stormwater outflows (F_p). In other words, system performance improves overall with increase hydronic flowrates, although the returns are diminishing.

Performance was degraded when 50% glycol replaced water as the heat transfer fluid in the geothermal system without making any other changes to the system. This was because the hydronic flowrate of the system decreased and shifted performance to a less optimal operating point, and because the thermal resistance of the SHX and GHX both increased.

There are simple solutions to both issues that would allow a geothermal system utilizing a 50% glycol solution to achieve equivalent performance to one using water: (i) use a larger pump with greater pumping power to increase the flowrate and (ii) increase the size of the SHX and GHX. Recall that in Equation 2 and Equation 4, the heat transfer is governed by the ratio of the heat exchanger length and the thermal resistance. It follows that *an increase in the thermal resistance could be counteracted* by a corresponding increase in the heat exchanger length to achieve equivalent heat transfer. In this study, this was not done because the budget put a constraint on the size of the GHX, the vault placed a constraint on the size of an SHX based on HDPE pipe , and the off-grid system placed a constrained on the pumping power that could be achieved on a continuous basis.

A final option to freeze-protect the system while requiring smaller changes to the component sizing is to use an ethanol heat transfer fluid instead of propylene glycol. It has a much lower viscosity compared to propylene glycol and the resulting issues can then the avoided. It is also non-toxic, like propylene glycol. Ethanol was not used in this study because it is flammable and has a flashpoint that was below the working temperatures in the mechanical enclosure. A potential risk was that an ethanol leak combined with a spark from the electrical equipment could create a fire hazard. This risk would need to be considered in the system design.

3.7 System Model Summer 2020

With the updated values for R_{SHX}, R_{GHX}, and T_g, all the parameters required for the model (Equation 9) to solve for T_{p2} were known. The modeled value of T_{p2} could then be compared against the actual measured value. However, there are two important things to note.

Firstly, the vault itself introduced some level of cooling. The walls and floor of the vault are in direct contact with the surface ground that is at a cooler temperature then the stormwater. The cooling capacity from the hydronic measurements (upon which the model is calibrated) includes only the geothermal contribution to the cooling where the actual T_{p2} measurements include both the geothermal and vault components of the cooling. The model ought to then predict that T_{p2} is going to be higher than was measured.

Secondly, at the beginning of August, the sensor for T_{p2} started reading erroneous values. At initial inspection, the readings looked reasonable. The actual measurements of T_{p1} and T_{p2} are shown in Figure 3-18. Note that the monitoring started late and missed the first half of June. T_{p2} suggests there is some level of cooling that is occurring as was expected. However, when capacity was plotted (Figure 3-19) it was clear that there was an issue with the T_{p2} data – starting in early August, the cooling appeared unrealistically large and furthermore, there appeared to be a large amount of cooling even when the system was off (i.e. when "Hydronic Measurements" is zero).

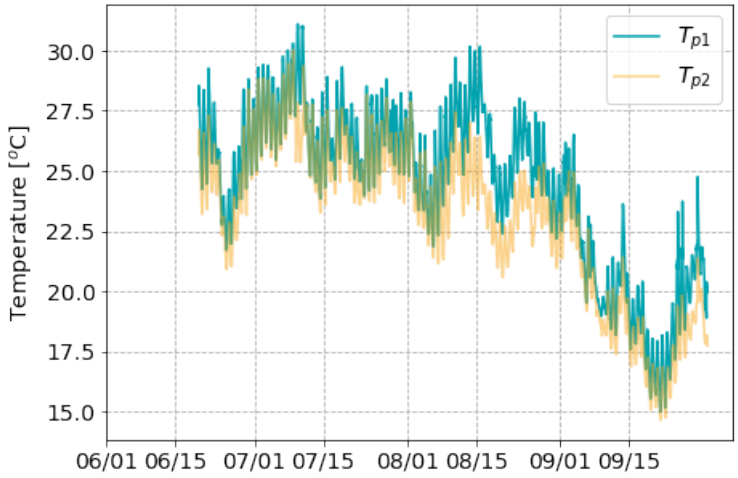

Figure 3-18. The measurements of T_{p1} and T_{p2} show that there is cooling occurring that, upon initial inspection appeared reasonable.

The data errors were a result of the T_{p2} sensor dislodging from its mounting and reading a combination of water temperatures and vault air temperatures. To evaluate the model, only the data from June and July 2020 could be used.

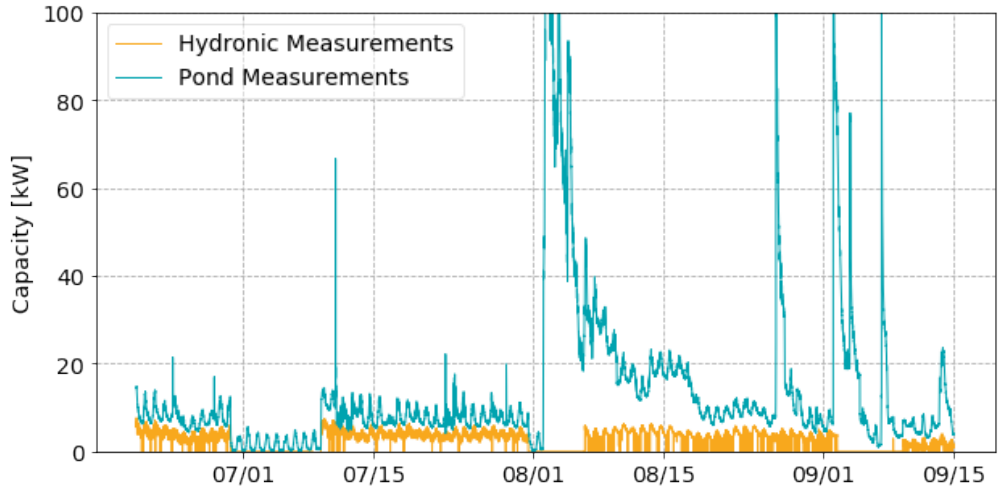

Figure 3-19. An error was observed when plotting the cooling capacity as a time series. The amount of cooling was much larger starting in early August, and there was cooling observed even when the geothermal system was off and the hydronic measurements showed zero capacity.

System data for a week in July is shown in Figure 3-20. Also shown is the predicted value of T_{p2} from the calibrated system model for comparison against the measured value of T_{p2}. Up to 4 °C of cooling was observed. The temperature difference between upstream and downstream is greatest for low flows, and the temperature upstream and downstream converge for low flows – as expected. However, the model predicts that only about half the cooling can be attributed to the geothermal system and the remainder attributed to the vault.

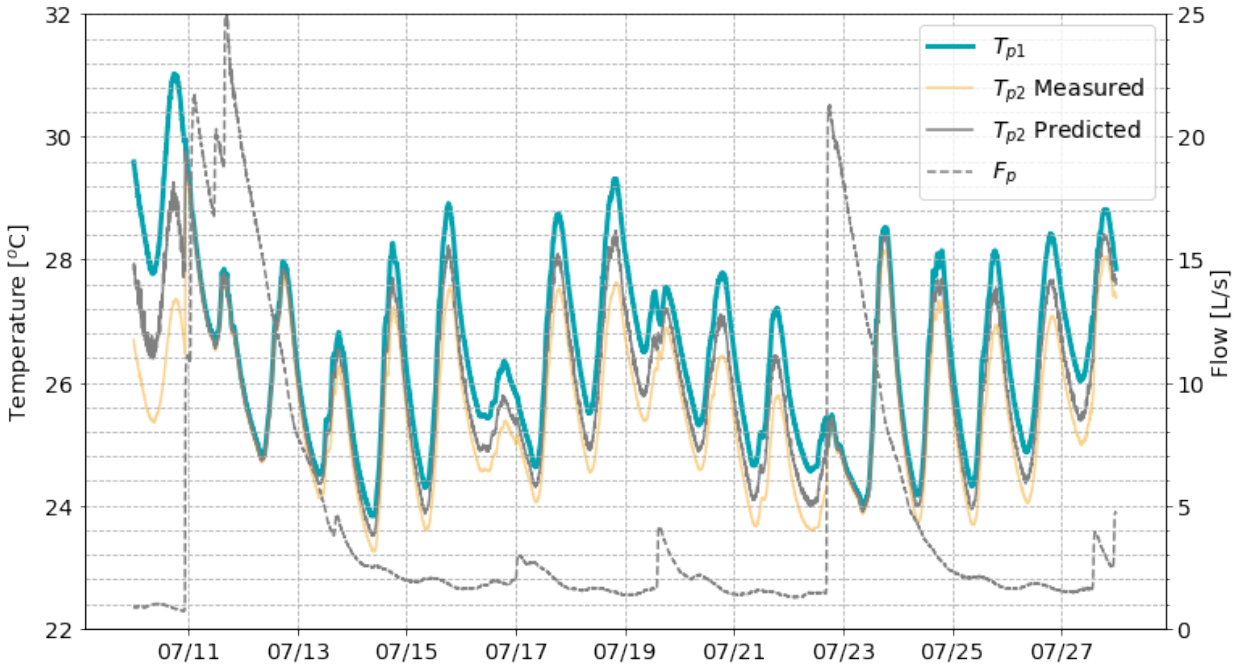

Figure 3-20. The predicted and measured value of T_{p2} is compared over more than two weeks in July. The temperature difference between measured and predicted is attributed to the cooling provided by the vault itself.

This prediction can be compared against the measured upstream and downstream temperatures when the system was off for a ground temperature measurement. Data from when the system was turned off in June/July (immediately preceding Figure 3-20) is shown in Figure 3-21. When the pond flow rate was approximately 1.25 L/s and the upstream temperature was approximately 29 °C, the vault itself was providing 0.6 °C of cooling. A similar data point from Figure 3-20 ("07/19") attributed 0.8 °C of cooling to the vault (the contribution of the vault is the difference between measured and predicted) – showing reasonably good agreement.

The relative contribution of the vault and the geothermal system for cooling can also be evaluated by plotting the cooling capacity as determined by the pond measurements (Equation 1), which included cooling from both geothermal and the vault, against the cooling capacity determined from the hydronic measurements (Equation 10), which includes only geothermal. This was done both for Summer 2019 and Summer 2020 in Figure 3-22. Note that data was aggregated over 12-hr periods to reduce the scatter. The plot shows that, in 2019, every 1 kW of cooling provided by the geothermal system is accompanied by 0.55 kW from the vault. In 2020, the relationship is 1:1. This is simply because the cooling capacity is lower when using the 50% glycol as the heat transfer fluid.

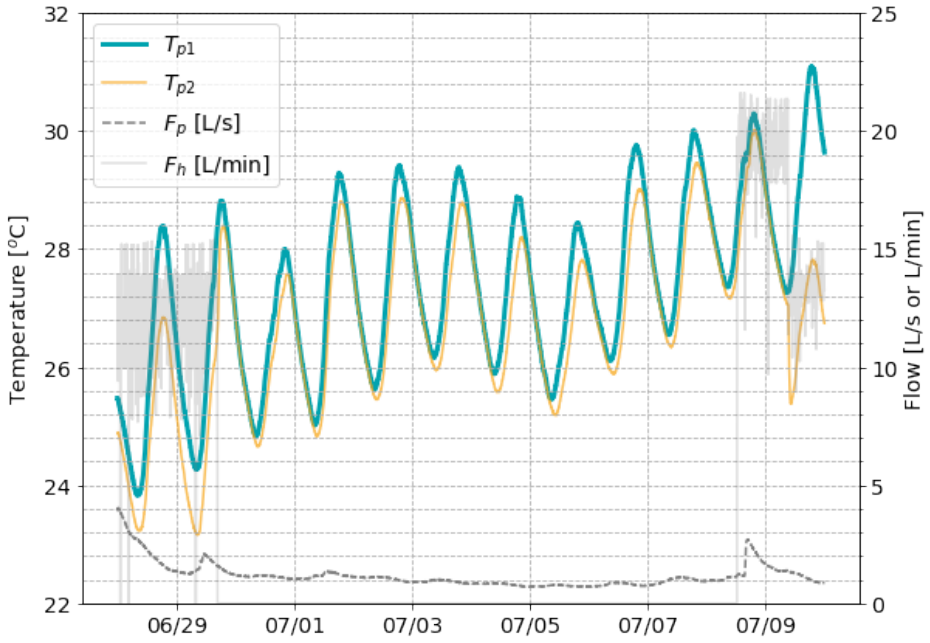

Figure 3-21. The upstream and downstream temperatures are shown for a period of time when the system was turned off (when the hydronic flowrate is zero). During this time a temperature difference up to 0.6 °C was achieved. This was due to cooling from the vault itself. Note that it is not a sensor offset error. Figure 3-20 shows that under high flowrates (where there is not enough cooling capacity to reduce the outflow temperature) the temperature sensors readings converge indicating they are well-matched.

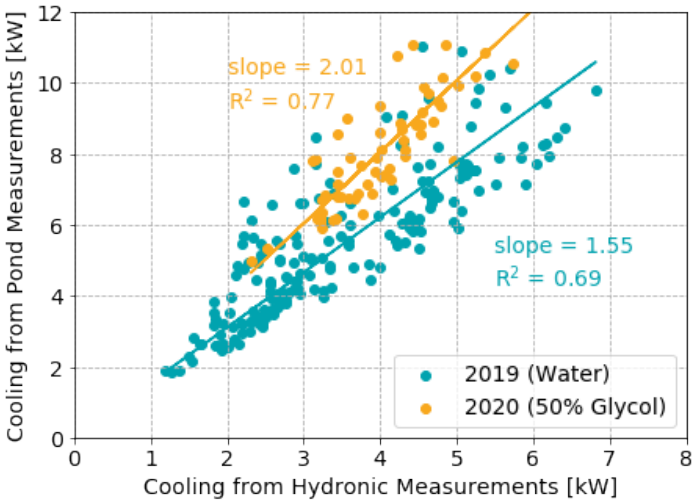

Figure 3-22. The relative contributions of the vault and the geothermal system are made clearer by plotting the cooling calculated from the pond measurements (which includes both the vault and the geothermal system) against the measurements from the hydronic systems (which includes only the geothermal system). The plot shows that, in 2019, every 1 kW of cooling provided by the geothermal system is accompanied by 0.55 kW from the vault. In 2020, the relationship is 1:1.

Figure 3-23 examines the accuracy of the model at predicted the cooling capacity of the geothermal system. The predicted capacity is calculated from predicted value of T_{p2} (Figure 3-20) used in Equation 1. The actual capacity is that determined from the hydronic measurements (Equation 10). The model tends to predict that the capacity is 4% higher than was achieved in practice (i.e. the slope is 1.04). The coefficient of determination (R^2) is high – indicating that the model is good at explaining the variation that was observed in the measured data.

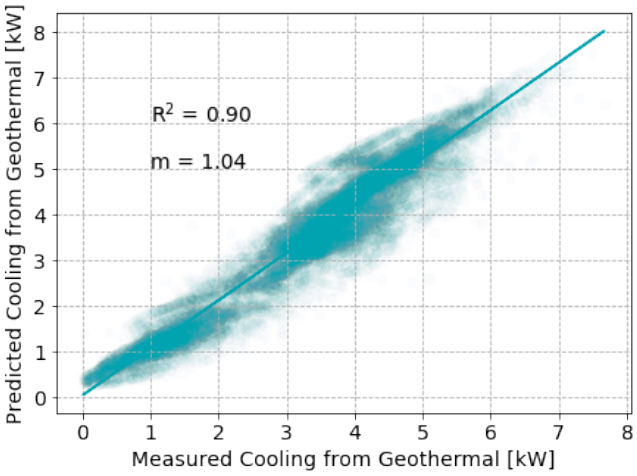

Figure 3-23. The accuracy of the calibrated geothermal system model was determined by comparing the predicted capacity against the hydronic measurements (which do not include the vault contributions to cooling). The model was a good predictor of actual geothermal system cooling capacity.

3.8 System Sizing

The ground temperature model, the calibrated system model, and the pond outflow and temperature data from both 2019 and 2020 were used for system sizing. The sizing considered the fraction of time across the summer (June 1st to September 15th for 2019, but June 18th to September 15th for 2020 due to data loss) that the downstream temperature was below 24 °C versus the number of deep vertical boreholes of the system. When using water as the heat transfer fluid, R_{GHX} and R_{SHX} were assumed to be 0.21 m°C/W and 0.17 m°C/W, respectively. For both water and propylene glycol, L_{SHX}, L_{GHX}, and F_h increased in integer multiples of 183 m, 230 m, and 17.4 L/min, respectively (the integer being the number of boreholes). When using propylene glycol as the heat transfer fluid, R_{SHX} was calculated using the model shown in Figure 3-15 and R_{GHX} was assumed to be 0.25 m°C/W based on Figure 3-11 and the hydronic flowrate.

Results are in Figure 3-24. Summer 2020 had a more significant thermal load than Summer 2019, although it appears to be worse in Figure 3-24 then it actually was due to the fact that data from early June is missing for Summer 2020. In Summer 2020, a geothermal system consisting of 10 deep vertical boreholes could keep outflow temperatures below 24°C for 91% of the time if using glycol, and 95% of the time if using water as the heat transfer fluid. With no geothermal the pond outflow temperatures would be below 24 °C only 25% of the time. In Summer 2019, approximately 6 deep vertical boreholes would keep outflow temperatures below 24 °C 95% of the time when using glycol, or 97% when using water as the heat transfer fluid.

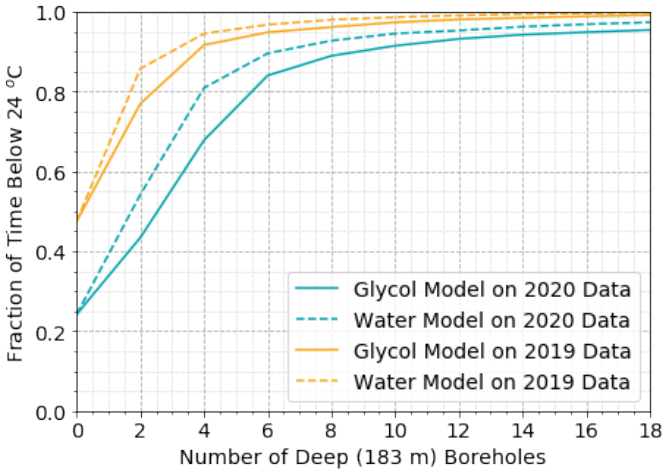

Figure 3-24. The ground temperature model, calibrated system models, and pond outflow data from 2019 and 2020 were used to model the impact of different geothermal system sizes on the outflow temperatures over the course of the summer.

4.0 DISCUSSION

A geothermal cooling system for a stormwater retention pond must use an anti-freeze solution within the hydronic circuit because a portion of the geothermal system would be above ground during the winter. Different antifreeze solutions are possible, including ethanol and propylene glycol. Both are non-toxic. Ethanol has superior heat transfer properties for this application because the viscosity of propylene glycol causes a reduction in performance. However, ethanol also has a low flashpoint at the concentrations required and this presented a potential fire hazard that the research team opted to avoid by instead using 50% propylene glycol.

Water was used as the heat transfer fluid in the system during the monitoring which took place in Summer 2019. Glycol replaced water prior to Winter 2019/2020 and monitoring continued with the glycol heat transfer fluid for Summer 2020. The aim of this addendum was to evaluate the change in performance and system sizing when using the glycol solution.

Ultimately, cooling capacity was poorer with glycol. This because thermal resistance of both the SHX and the GHX increased, and the overall flowrate through the system was reduced. The data showed correlations between R_{SHX} and the glycol temperature, and also between R_{GHX} and the hydronic flowrate. The driving force behind these correlations was believed to be the viscosity of glycol, which changes notably over the relatively small range of hydronic temperature occurring within the system over the course of the summer. The system parameters under normal conditions for both glycol and water are summarized below in Table 4-1.

Table 4-1. Change in heat exchanger thermal resistances between water and glycol heat transfer fluids.

	Water	**50% Glycol**
R_{SHX} [m°C/W]	0.17	0.17 – 0.27
R_{GHX} [m°C/W]	0.21	0.25

While the use of glycol does increase the thermal resistance of the SHX and GHX, it is important to recall from Equation 2 and Equation 4, that the heat transfer is governed by the ratio of the heat exchanger length and the thermal resistance. It follows that *an increase in the thermal resistance could be counteracted* by a corresponding increase in the heat exchanger length to achieve equivalent heat transfer. In other words, comparable levels of cooling capacity are possible when use glycol or water as a heat transfer fluid, but with glycol the SHX and GHX would just need to be larger.

When it comes to calculating the system size required to reach a certain target (for example, 90% or 95% of the outflow temperatures below some set-point value) the difference between the two heat transfer fluids becomes much lower. This is because much of the thermal load is more constant "background" thermal load occurring when the pond is slowly draining in the inter-events periods, and a small fraction of the thermal load are peaks that a system would struggle to manage regardless of the heat transfer fluid. To reach a target of >90% the system is already oversized for the majority of the thermal load of the pond. If a system is oversized for the majority of the thermal load then it matters less that a system using glycol has less capacity then one with water because it can still has *enough* capacity to reach the set-point target. That helps explains why the glycol and water curves converge in Figure 3-23.

As outlined in the *Interim Report*, the need remains for additional thermal mitigation measures to keep outflows within target values a greater percentage of the time. Infiltration, in particular, requires re-examining. The modeling in this addendum showed that the floor and walls of the concrete vault containing the stormwater heat exchanger provided a notable amount of cooling. This is because the vault is in contact with the cooler subsurface ground and the interior of the vault is also shaded from solar radiation. These two features allow a vault to be potentially more

impactful at cooling than rock-filled cooling trenches that are often deployed. In a sense, the vault is also providing "geothermal" cooling in that it is transferring heat from the stormwater to the subsurface ground, just that the vault is "passive" (no hydronics or pumping) and it there is a smaller temperature differential to drive heat transfer.

For a concrete vault to provide to a significant level of cooling it would need to be several times larger than the vault installed at the pilot pond, and this may not be feasible due to either space or cost constraints. However, a large underground infiltration chamber could have a similar cooling impact to a vault, in addition to infiltrating the stormwater. When considering an infiltration chamber, the *Interim Report* concluded that such a chamber would need to be prohibitively large to make a significant impact on the thermal load and that the other measures considered, longer drawdown times and subsurface draw, would be more impactful. This needs re-examination. The *Interim Report* only considered the impact of an infiltration chamber mitigating the flowrates from the pond. It did not consider passive heat transfer between the warm stormwater and the cool subsurface ground (like that occurring in the vault). The latter factor may be the most important regarding thermal mitigation. This should be considered in future work.

A final point to note is that the thermal load from the pond in 2020 was much than that in 2019, and it was also high compared to previous years considered in this study. To effectively size a system, one needs to know (or estimate) the thermal load. The *Interim Report* found that a machine learning model that incorporated both rain and temperature data was sufficient to estimate the thermal load of the pond. This approach requires monitoring data from at least one season. It could be used to project the thermal load moving forward (rather than only considering historical data) since the thermal load is expected to increase with climate change.

Additional considerations, like improvements in the heat exchangers, integration with other thermal mitigation approaches, system costs, and future work are discussed in the *Interim Report*.

5.0 CONCLUSION

This addendum compared the performance of a geothermal cooling system for a stormwater retention pond when using different heat transfer fluids. The system was not designed to meet the full load of the pond. Rather, it was a small-scale pilot that was used to model and understand system performance such that a full-scale system could be sized. In Summer 2019, the system used water. In Summer 2020, the system used 50% propylene glycol which was required to freeze-protect the system as it sat outside over the winter. Data monitoring and analysis was performed for both seasons.

The glycol caused an increase in the thermal resistance for both the ground and stormwater heat exchangers, which then caused a large reduction in overall cooling capacity for the system. The reduction in performance varied with the stormwater outflow temperature (the reduction being smallest at warmer temperatures) and was on the scale of 20% to 40%. The data was used to calibrate a system model and the model was then used to evaluate the impact of different system sizes on the stormwater temperatures downstream of the geothermal system.

The impact of the glycol solution was less pronounced in the overall system sizing. In Summer 2020, a geothermal system consisting of 10 deep vertical boreholes could keep outflow temperatures below 24°C for 91% of the time if using glycol, and 95% of the time if using water as the heat transfer fluid. With no geothermal, the pond outflow temperatures would be below 24 °C only 25% of the time. In Summer 2019, approximately 6 deep vertical boreholes would keep outflow temperatures below 24 °C ~97% when using water as the heat transfer fluid, or 95% with water as the heat transfer fluid.

In the landscape of thermal mitigation technologies, an "active" geothermal system like that studied in this project offers something unique. Amongst other benefits, it can provide a large amount of cooling capacity in a small volume. It is also an approach that is highly adaptable to the existing site constraints. For example, a stormwater heat exchanger could be installed within the aggregate of an underperforming cooling trench, or similarly it could be installed in a stormwater outflow pipe. For similar reasons, active geothermal ought to integrate well with other thermal mitigation measures in the context of both an existing and in a new pond.

"Passive" systems (i.e. no hydronics or pumping) are normally preferred, but they may not always be feasible or may not have sufficient cooling capacity to meet target outflow temperatures. In those circumstances, this pilot has demonstrated that geothermal offers a compelling option. Additional considerations on system improvements, sizing, future work, and other topics are available in the *Interim Report*.